Chem

CellPress

Article

Plasmon-Induced Interfacial Hot-Electron Transfer Directly Probed by Raman Spectroscopy

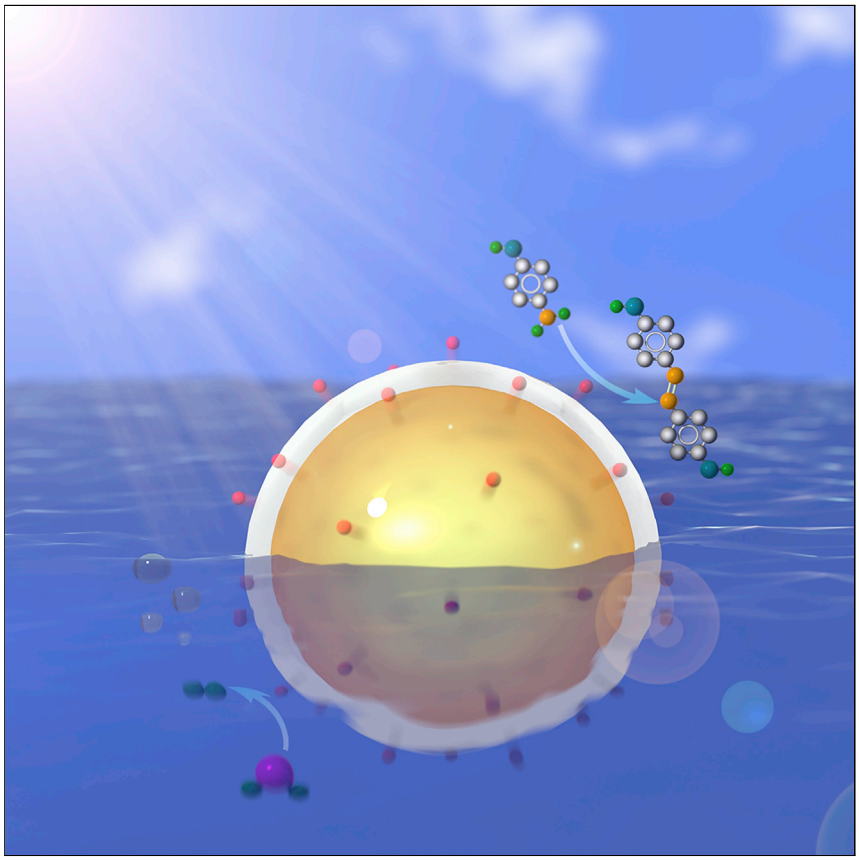

Plasmon-mediated photocatalysis via hot-electron transfer has attracted increasing interest recently. However, the interfacial hot-electron transfer mechanism and how it affects photocatalysis are still not completely understood. Herein, the plasmon-induced hot-electron transfer at different plasmonic interfaces is investigated *in situ* at a (sub)nanometer level. It is found that hot electrons can migrate across the Au-semiconductor or Au-metal interfaces and transfer more than 10 nm in semiconductors but less than 1 nm in metals.

Hua Zhang, Jie Wei, Xia-Guang Zhang, ..., Feng Pan, Zhong-Qun Tian, Jian-Feng Li

li@xmu.edu.cn

HIGHLIGHTS

Hot-electron transfer at different interfaces is probed at a (sub) nanometer level

Hot electrons can go more than 10 nm in semiconductors but less than 1 nm in metals

Role of hot-electron transfer on photocatalysis and photoelectrocatalysis is revealed

Zhang et al., Chem 6, 689–702
March 12, 2020
https://doi.org/10.1016/j.chempr.2019.12.015

Chem

CellPress

Article

Plasmon-Induced Interfacial Hot-Electron Transfer Directly Probed by Raman Spectroscopy

Hua Zhang,[1] Jie Wei,[1] Xia-Guang Zhang,[1] Yue-Jiao Zhang,[1] Petar M. Radjenovica,[1] De-Yin Wu,[1] Feng Pan,[2] Zhong-Qun Tian,[1] and Jian-Feng Li[1,3,*]

SUMMARY

Plasmon-mediated photocatalysis via hot-electron transfer attracts increasing interest due to its capability to improve energy utilization efficiency. However, more insightful information is still needed to reveal the mechanism of interfacial hot-electron transfer. Herein, the plasmon-induced hot-electron transfer at different plasmonic interfaces, including Au-insulator (SiO_2), Au-semiconductor (TiO_2 and Cu_2O), and Au-metal (Pd and Pt), is directly investigated using surface-enhanced Raman spectroscopy (SERS) and density functional theory calculation with a (sub)nanometer spatial resolution, through the fabrication of well-defined plasmonic nanostructures. (Sub)nanometer-distance dependence of interfacial hot-electron transfer has been identified for the first time. Hot electrons can migrate across the Au-semiconductor or Au-metal interfaces and transfer more than 10 nm in semiconductors but decay to thermally equilibrated states rapidly in metals in less than 1 nm. Such a transfer process is blocked at the Au-insulator interface. This work promotes the fundamental understanding of plasmon-induced hot-electron transmission and photocatalysis at plasmonic interfaces.

INTRODUCTION

Solar energy, because of its worldwide availability and renewable nature, is becoming the most promising energy resource for the future. Storage and conversion of solar energy into chemical energy via photocatalytic processes has attracted much interest since the pioneering work by Fujishima and Honda.[1] Extensive effort has been applied to improve the energy utilization efficiency of photocatalysis by optimizing photocatalysts.[2] A few strategies have been developed to achieve this goal, such as improving the light-absorbing efficiency of semiconductors,[3] accelerating the separation of photogenerated electron-hole pairs,[4] and tuning the properties of cocatalysts.[5] However, the performances of most photocatalytic processes are still low and need to be further improved to make them commercially viable and industrially scalable.

Recently, localized surface plasmon resonance (LSPR) of metallic nanomaterials has attracted increasing interest and has been used to improve the efficiency of various photocatalytic processes.[6–8] LSPR refers to the resonant collective oscillation of the valence electrons of nanomaterials when being excited by an incident light source whose frequency matches the natural frequency of oscillating surface electrons.[9] As the resonant wavelength and LSPR intensity of a metal depend on its composition, size, morphology, and structure, it is possible for a photocatalyst to interact with

The Bigger Picture

Plasmonic materials like Au, Ag, and Cu nanostructures can generate energetic hot electrons when being excited by a suitable incident light. Such hot electrons would be transferred to other materials and greatly boost photocatalytic processes occurring there. However, the hot-electron transfer mechanism and how it affects photocatalysis is still not completely understood, greatly hindering the rational design of efficient plasmonic photocatalysts. Herein, the transfer of hot electrons at Au-metal, Au-semiconductor, and Au-insulator interfaces, as well as its role on plasmon-mediated photocatalysis and photoelectrocatalysis, is investigated using *in situ* Raman spectroscopy. Furthermore, the spatial distance that hot electrons can go in metals and semiconductors is unveiled at a (sub)nanometer level. Such a fundamental study provides guiding insights for the development of efficient plasmonic photocatalysts.

sunlight in the entire solar spectrum by manipulating these factors.[10] Therefore, various LSPR-type photocatalysts and photocatalytic processes have been developed over the last decade. For example, plasmonic nanomaterials under light illumination can directly activate H_2, O_2, etc., thus, advancing hydrogenation or oxidation reactions.[11–14] They can also form nanocomposites with semiconductors and extend their light absorption spectra.[15–19] Furthermore, plasmonic nanomaterials can affect the catalytic properties of cocatalysts such as Pt and Pd nearby so that the activity or selectivity of the cocatalysts can be enhanced.[20–22]

Different mechanisms have been proposed to explain the plasmon-enhanced photocatalysis.[7,23,24] Among them, the hot-electron transfer mechanism has attracted the most attention. Plasmonic nanomaterials can generate hot electrons that have energies much higher than those at the thermal equilibrium state. The generated hot electrons can be transferred either into the frontier orbital of reactants or the conduction bands of semiconductors. Therefore, hot electrons can drive reactions that cannot be achieved via other conventional methods, such as heating etc., opening up new reaction pathways for the chemical industry.[25] Such a hot-electron transfer process at plasmonic interfaces, especially plasmonic metal-semiconductor interfaces, was demonstrated using time-resolved spectroscopy, Schottky diodes, or even density functional theory (DFT) simulations.[18,26–28] However, a fundamental understanding of the plasmon-induced interfacial hot-electron transfer and how it affects photocatalysis is still lacking, which significantly limits the development of more efficient LSPR-type photocatalysts.

One way to solve this significant puzzle is using spectroscopic techniques to monitor the reaction processes to uncover the fundamental insights of the plasmon-enhanced photocatalysis. Of the spectroscopic techniques available, Raman spectroscopy holds great potential as it can provide "fingerprint" structural information. Furthermore, the plasmonic materials used in plasmon-mediated photocatalysis can also generate strong and highly localized electromagnetic fields that can significantly enhance the Raman signals of molecules nearby, leading to the well-known surface-enhanced Raman spectroscopy (SERS).[29,30] SERS is extremely sensitive and can even achieve the detection of single molecules, making it a promising tool for the *in situ* study of catalysis with excellent sensitivity and high spatial resolution.[31,32] Therefore, it offers unprecedented opportunities for the in-depth exploration of plasmon-induced hot-electron transfer, as well as plasmon-enhanced photocatalysis, via tactful design and manipulating LSPR-type photocatalysts that allow *in situ* SERS study and plasmon-enhanced photocatalysis simultaneously.

Herein, the transmission of hot electrons, generated on the Au nanoparticles, in various materials, including insulators (SiO_2), semiconductors (TiO_2 and Cu_2O), and metals (Pd and Pt), and its influence on the photocatalytic conversion of para-aminothiophenol (pATP) and photoelectrochemical water splitting was directly investigated at a (sub)nanometer level using *in situ* SERS and DFT calculations. It is found that photogenerated hot electrons could only be transferred from Au to semiconductors or metals, but would be blocked at the Au-insulator interface, due to the very different electronic structures at these plasmonic interfaces. Furthermore, the distance that hot electrons can go in semiconductors or metals is very different. Hot electrons can travel more than 10 nm in semiconductors, but less than 1 nm in metals, to the surface and mediate the photocatalytic reaction occurring there.

[1]College of Materials, State Key Laboratory of Physical Chemistry of Solid Surfaces and College of Chemistry and Chemical Engineering, College of Energy, Fujian Key Laboratory of Advanced Materials, Xiamen University, Xiamen 361005, China

[2]School of Advanced Materials, Peking University, Shenzhen Graduate School, Shenzhen 518055, China

[3]Lead Contact

*Correspondence: li@xmu.edu.cn

https://doi.org/10.1016/j.chempr.2019.12.015

RESULTS

Fabrication of the Gap-Mode Configuration Allowing Plasmon-Enhanced Photocatalysis and *In Situ* SERS Study Simultaneously

A gap-mode configuration was employed to explore the transmission of hot electrons in various materials (Figures 1A and 1B). pATP was first assembled on a Au(111) single crystal surface that has an atomic flat surface structure (Figure 1C), so that the influence of the roughness of the underlying substrate is excluded and all the molecules are located at the same horizontal position. Core-shell nanoparticles, composed of Au-core nanoparticles coated with different material shells, were deposited on the Au(111) surface and were used to catalyze the conversion of pATP to p,p′-dimercaptoazobenzene (DMAB). This reaction has been postulated to be driven by hot electrons[33] and is an important probe reaction in SERS, tip-enhanced Raman spectroscopy (TERS), Raman imaging, etc.[34,35] If the hot electrons generated on the Au cores can be transferred into the shells then pass through the shells, they will likely react with pATP, leading to the formation of DMAB. Therefore, transmission of hot electrons in different plasmonic interfaces and materials can be easily studied by changing the composition and thickness of the shells.

The Au(111) single crystal surface was prepared in a hydrogen-oxygen flame via the well-established Clavilier method and shows a well-defined surface structure (Figure 1C). A monolayer of pATP was first assembled on the Au(111) single crystal surface. The as-prepared bare Au nanoparticles (~55 nm, Figure S1) were then deposited on the pATP assembled surface, forming a submonolayer structure (Figure 1D). As Au(111) cannot generate hot electrons directly, all the hot electrons participating in the photocatalytic conversion of pATP come from the Au nanoparticles, allowing the study of the transfer of hot electrons using core-shell nanoparticles.

Figure 1E displays the SERS spectra of such a Au/pATP/Au(111) gap-mode structure under the excitation of a 633 nm laser. The characteristic pATP Raman peaks located at ~1,000, ~1,080, and 1,178 cm^{-1}, attributed to the benzene ring bending mode and the C–S (ν_{C-S}) and C–N (ν_{C-N}) stretching modes, respectively,[33] are clearly observed because of the strong Raman enhancement generated by the Au nanoparticles. Also, three additional peaks located at 1,140, 1,392, and 1,445 cm^{-1} are observed. These peaks can be assigned to the C–N and N=N stretching vibrational modes of DMAB.[33,36] We find that the yield of DMAB can be tuned by changing the Au size (see Figure S2 and the corresponding discussion for details), which is well consistent with previous studies.[37] It has also been reported that the yield and selectivity of DMAB can be further improved by changing the shape of Au nanoparticles, adding some metal cations, applying an external electric field, or manipulating the incident light.[38–41] According to previous studies,[36,42] the formation of DMAB is catalyzed by the hot electrons generated by the Au nanoparticles.

To confirm that the conversion of pATP to DMAB is triggered by hot electrons generated in the Au nanoparticles, we then studied the conversion of pATP with different laser powers. With increasing laser power, the relative intensity of DMAB to that of pATP also increases, though all the Raman peaks increase rapidly (Figure 1E), clearly demonstrating that this reaction is activated by light. We have also investigated the influence of plasmon heating on this reaction, as the temperature of the samples would be increased under illumination. To avoid the interference of the laser, a very low laser power (~10 μW) and a defocusing strategy were applied in this experiment. Under such conditions, the yield of DMAB is rather low and only slightly

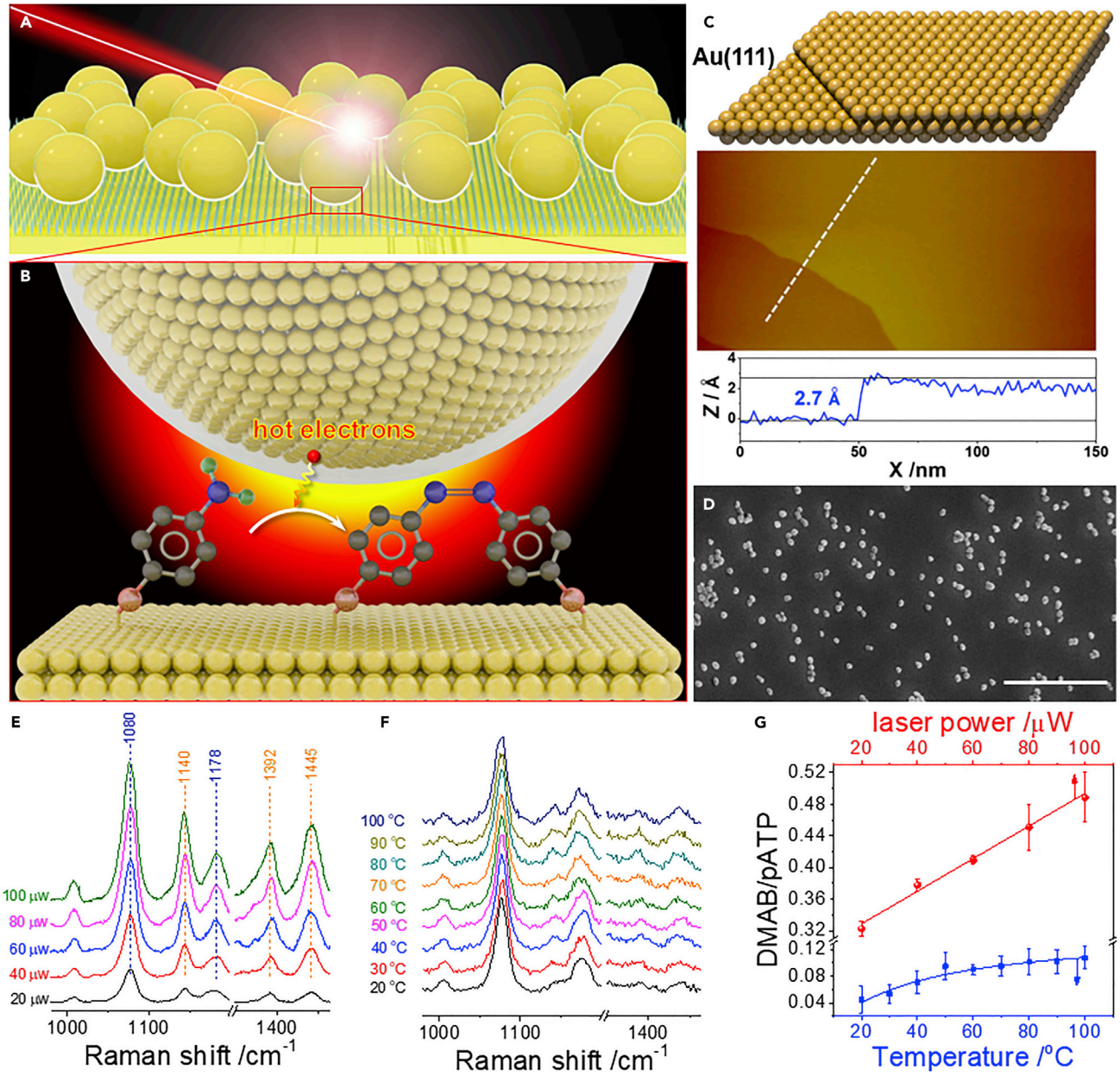

Figure 1. *In Situ* SERS Study of the Plasmon-Induced Hot-Electron Transfer at Different Plasmonic Interfaces

(A and B) Schematic illustration of *in situ* SERS study on the interfacial transmission of hot electrons using the photocatalytic conversion of pATP to DMAB as a probe reaction.

(C) Schematic and scanning tunneling microscopy (STM) image of the Au(111) single crystal surface. The STM image was obtained using a Pt-Ir tip with a dimension of 150 × 300 nm^2. The bottom panel shows the height profiles corresponding to the white dashed line in the STM image.

(D) SEM image of a submonolayer of Au nanoparticles on Au(111). Scale bar, 1 μm.

(E) SERS spectra of the conversion of pATP catalyzed by bare Au nanoparticles under different incident laser powers. Excitation laser, 633 nm; exposure time, 10 s, and temperature: 20°C.

(F) SERS spectra of the conversion of pATP catalyzed by bare Au nanoparticles at different temperatures. Excitation laser, 633 nm; exposure time, 10 s; laser power,10 μW; and a defocusing strategy was applied to avoid the interference of the laser.

(G) The relative intensity of DMAB to pATP bands under different incident laser powers and temperatures.

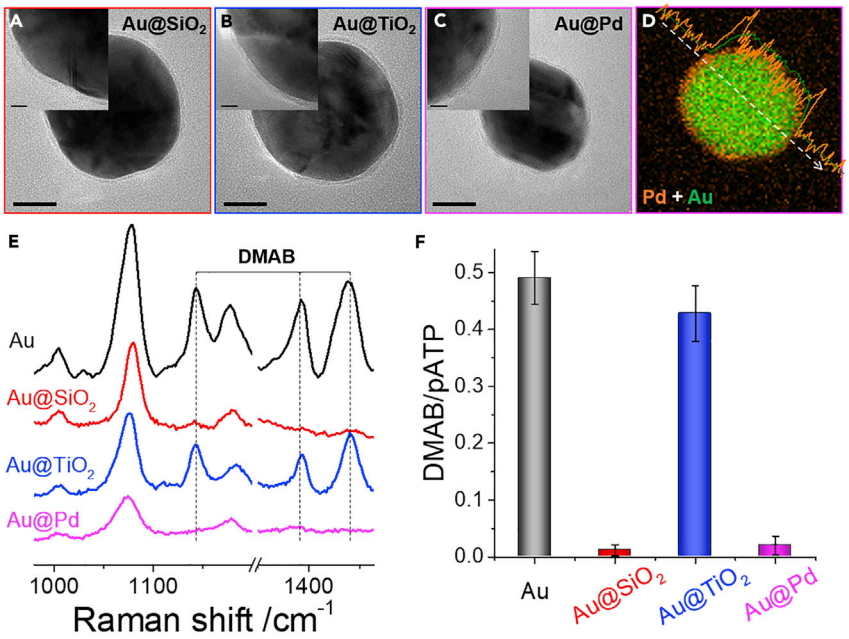

Figure 2. Photocatalytic Conversion of pATP Using Different Core-Shell Nanoparticles

(A–C) TEM images of $Au@SiO_2$, $Au@TiO_2$, and Au@Pd, respectively. Scale bars, 20 nm and 5 nm for the insets.

(D) Elemental maps and line scan analysis of Au@Pd.

(E) SERS spectra of the conversion of pATP adsorbed on Au(111) catalyzed by different core-shell nanoparticles. Excitation laser, 633 nm; laser power, 0.1 mW; and exposure time, 10 s.

(F) Relative Raman intensity of DMAB to pATP for different nanostructures.

increases with temperature (Figure 1F). The quantitative results in Figure 1G illustrate that the yield of DMAB displays a linear relationship with the laser power, which is a typical signature of hot-electron-driven chemical reactions,[12] but an exponential relationship with temperature. These results are consistent with previous studies and clearly confirm that the plasmon-mediated conversion of pATP to DMAB is a hot-electron-driven reaction, though a plasmon heating effect can slightly improve the efficiency.[43–45]

Hot-Electron Transfer at Different Plasmonic Interfaces

To investigate the transmission of hot electrons at different plasmonic interfaces, nanostructures with Au cores and different shells were then prepared via seed-mediated methods (see the Supplemental Information for detailed synthesis procedures). SiO_2, TiO_2, and Pd, as representative examples of insulators, semiconductors, and conductors, respectively, were coated on the Au-core nanoparticles. TEM images along with the energy dispersive X-ray (EDX) spectra clearly show that these materials were successfully coated on the Au nanoparticles, forming homogeneous shells with thicknesses of around ~2 nm (Figures 2A–2C and S3). The scanning transmission electron microscopy (STEM)-EDX elemental mapping and line scan analysis further demonstrate the core-shell-like structure (Figure 2D). Our previous studies using SERS have well demonstrated that these materials could form complete shells on the Au nanoparticles,[46–48] thus direct contact between the Au cores and the probe molecules could be excluded. Furthermore, the UV-vis absorption measurement illustrates that the LSPR band of the Au cores only shift slightly to a higher wavelength after coating these ultrathin shells on them (Figure S4).

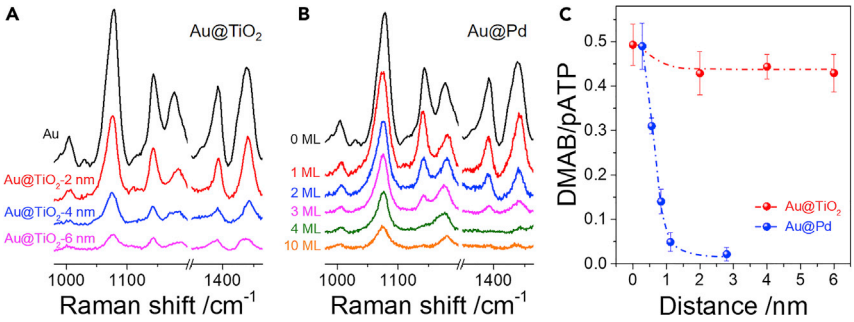

Figure 3. Influence of Shell Thickness on the Transmission of Hot Electrons

(A and B) SERS spectra of the conversion of pATP adsorbed on Au(111) catalyzed by $Au@TiO_2$ and Au@Pd with different shell thicknesses. Excitation laser, 633 nm; laser power, 0.1 mW; and exposure time, 10 s.

(C) Relative Raman intensity of DMAB to pATP as a function of the shell thickness.

The as-prepared core-shell nanoparticles were then deposited on the pAPT monolayer-assembled Au(111) single crystal surface to study the transmission of hot electrons at the plasmonic Au-shell interfaces. As for the insulator shell, i.e., $Au@SiO_2$, only the Raman peaks of pATP were observed under the irradiation of a 633 nm laser, while the formation of DMAB is almost completely inhibited (red curve of Figures 2E and 2F). Such a result is well consistent with previous studies[49] and demonstrates that the SiO_2 shell can block the transmission of hot electrons. Furthermore, it can also be inferred that the generation of hot electrons would not occur in Au(111) even in the presence of a plasmonic nanogap. However, when the shell was changed from an insulator to a semiconductor, i.e., $Au@TiO_2$, the three characteristic Raman peaks of DMAB appear again and the intensities relative to pATP are very similar to that for the bare Au nanoparticles (blue curve of Figures 2E, 2F, and S5). Furthermore, Figure S6 illustrates that no DMAB is formed for $Au@SiO_2@TiO_2$, which demonstrates that the conversion of pATP to DMAB does not result from the catalysis role of TiO_2 itself. Therefore, hot electrons generated by the Au core can migrate across the Au-TiO_2 interface and through the TiO_2 shell to its outer surface and drive the photocatalytic conversion of pATP to DMAB. More interestingly, when the Au nanoparticles were coated with Pd, an excellent electronic conductor, DMAB is also not observed (pink curve of Figures 2E and 2F). As the excitation light (633 nm) used here cannot stimulate the plasmonic effect on Pd whose LSPR band locates at the UV region, hot electrons would be generated in the Au cores and then transfer to the Pd surface. Therefore, such unexpected results illustrate that the hot electrons would not be transferred across the Pd shell.

Transmission Distance of Hot Electrons in Semiconductors and Metals

The distance that the hot electrons can transfer in TiO_2 and Pd was further investigated at a (sub)nanometer level by changing the thickness of the TiO_2 and Pd shells (Figure S7). As shown in Figures 3A and 3B, the intensity of all the Raman signals decreases rapidly with an increase in shell thickness due to the attenuation of the electromagnetic field at the Au(111) surface. However, DMAB can still be observed for $Au@TiO_2$ with thicker shells. Quantitatively, the yield of DMAB with $Au@TiO_2$ remains almost unchanged even when the shell thickness is increased to 6 nm (Figure 3C). Such results indicate that once the hot electrons are transferred into the TiO_2 shell, they would behave similar to the free electrons of TiO_2. As the mean free path of electrons in TiO_2 is about several tens of nanometers, these electrons can efficiently transfer to the surface and react with pATP there.

On the other hand, for the Pd shell, the formation of DMAB is strongly dependent on the shell thickness. 1–10 monolayers (MLs) of Pd was coated on the Au nanoparticles (1 ML of Pd is about 0.28 nm[50]). From Figure 3B, the yield for DMAB for Au@Pd-1 ML is similar to that for the bare Au nanoparticles. However, it declines significantly with increasing Pd shell thicknesses. The yield of DMAB for Au@Pd-2 ML is only ~60% of that for Au@Pd-1 ML and almost no DMAB is generated when 4 ML Pd is coated on the Au nanoparticles (Figure 3C). Such results clearly indicate that the hot electrons generated on Au can be transferred to the Pd shell via the Pd-Au interface but the distance that the hot electrons can go in Pd is < 1 nm, much shorter than in TiO_2. Furthermore, the influence of the Pd-Au interface on the transmission of hot electrons was also studied using Au-core Pd-satellite nanocomposites (Figure S8A), which have been frequently used as efficient catalysts for plasmon-mediated photocatalysis.[20,21,51] The quantity of the Pd-Au interfaces was manipulated by changing the density of the Pd nanoparticles on the Au nanoparticles (Figures S8B–S8E). It was clearly found that the relative intensity of DMAB to pATP significantly declined with an increase in the quantity of the Pd-Au interfaces (Figure S8F), directly demonstrating that the hot electrons generated on the Au nanoparticles would migrate to Pd via the Pd-Au interfaces.

To further compare the distance that hot electrons can transfer in semiconductors and metals, photocatalytic conversion of pATP to DMAB was also investigated using Au@Cu_2O and Au@Pt core@shell nanoparticles. As shown in Figure S9, Cu_2O, a typical semiconductor with a band gap smaller than that of TiO_2, is coated on Au nanoparticles, forming Au@Cu_2O core@shell nanoparticles with a shell thickness of ~5 and ~10 nm. Similar to Au@TiO_2, DMAB is clearly observed when the Au@Cu_2O nanoparticles are used in the photocatalytic conversion of pATP to DMAB. The relative intensity of DMAB to pATP remains almost unchanged when the thickness of the Cu_2O shell increases from 5 to 10 nm. Such results indicate that hot electrons generated on Au nanoparticles can be transferred to the Cu_2O shell and transfer more than 10 nm in Cu_2O. On the contrary, as for the Pt metal coated Au nanoparticles, the yield of DMAB is significantly decreased when the thickness of the Pt shell increases from 2 monolayers to 10 monolayers (Figure S10), further demonstrating that the distance that hot electrons can transfer in metals is much shorter than that in semiconductors. Such a result is also well consistent with the finite element method (FEM) simulations by Linic et al.[52] They found that the Au nanoparticles could not drive the transfer of the plasmonic energy into the Pt shells on them. But such energy transfer would occur at Ag-Pt interfaces, leading to the direct generation of hot electrons in Pt, thus complicating the hot-electron transfer behaviors at the interfaces.

Interfacial Hot-Electron Transfer Mechanism

To understand the transmission mechanism of hot electrons at plasmonic interfaces, DFT was further performed to determine the projected density of states (DOSs) of different interfaces (Figures 4A–4C). At the Au-SiO_2 interface, the SiO_2 overlayer displays a band gap of more than 4 eV. Such a value is much smaller than that of bulk SiO_2 (Figure S11A), indicating the existence of strong electronic interactions between the SiO_2 overlayer and the underlying Au. The bottom of the conduction band of the SiO_2 overlayer locates at ~4.2 eV (Figure 4C). Given that a 633 nm laser was used as the excitation light source, the maximum energy of the hot electrons generated by the Au nanoparticles is only about 1.9 eV. Therefore, these electrons are not "hot" enough to be transferred to the conduction band of the SiO_2 overlayer. In other words, the hot electrons cannot be transferred through the Au-SiO_2 interface.

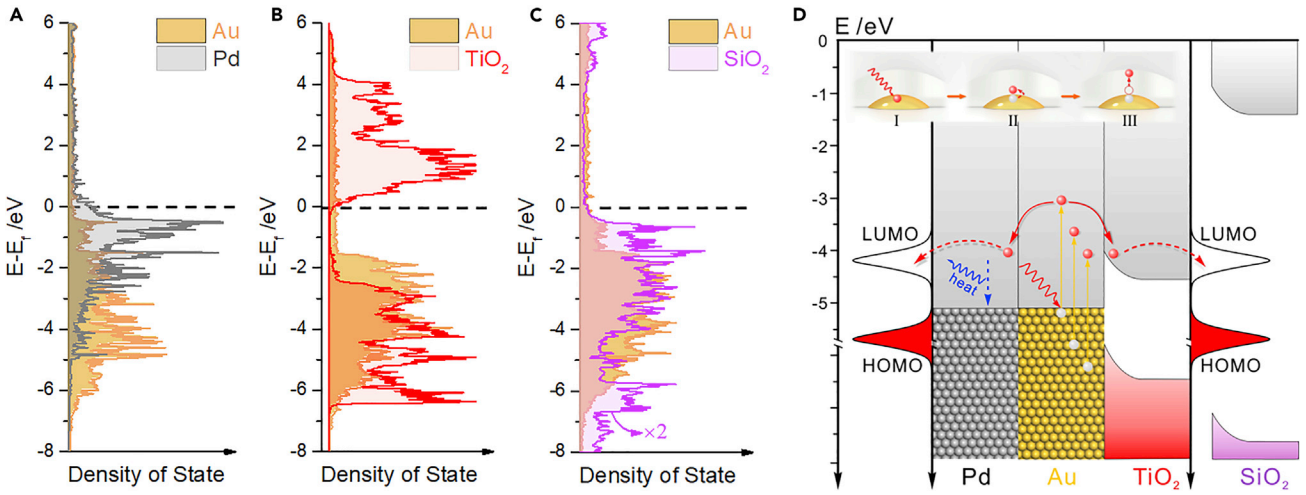

Figure 4. Mechanisms for the Transmission of Hot Electrons at Different Plasmonic Interfaces

(A–C) Projected DOSs for the Au-Pd, Au-TiO_2, and Au-SiO_2 plasmonic interfaces, respectively.

(D) Proposed mechanism for the transportation of hot electrons at the plasmonic interfaces. (1) generation of hot electrons at the Au nanoparticles, (2) transmission of hot electrons at the plasmonic interfaces, and (3) migration of hot electrons in the shell materials.

The DOS of the Au-TiO_2 interface is also calculated, which is very different from that of pure TiO_2 because of the electronic interaction between Au and TiO_2 (Figure S11B). As displayed in Figure 4B, the bottom of the conduction band of the TiO_2 overlayer is only slightly higher than the Au Fermi level and the DOS maximum is close to 1 eV. As a result, the photogenerated hot electrons would rapidly enter the conduction band of TiO_2 from Au via the Au-TiO_2 interface. Because of the Schottky barrier between TiO_2 and Au, hot electrons would have a much longer lifetime in TiO_2 than Au and can thus migrate similar to free electrons to the surface of the TiO_2 shell and drive photocatalytic reactions, as was observed.[9,53] Furthermore, as only the hot electrons with energy higher than the Schottky barrier can be transferred to TiO_2, the photocatalytic performance of Au@TiO_2 is slightly lower than that of bare Au nanoparticles.

Unlike SiO_2 and TiO_2, Pd is an excellent electronic conductor, thus the Pd overlayer displays a continuous electronic band structure and the DOS above the Fermi level is low. Hence, the hot electrons generated in the Au cores could easily be transferred to the Pd shell. However, due to its continuous electronic band structure, the lifetime of such electrons in Pd should be very short. As the thickness of the Pd overlayer increases, the hot electrons would rapidly decay to thermally equilibrated states via recombination with the hot holes, electron-electron interactions, or interacting with defects in Pd. Such a decay process can also be demonstrated by the higher local temperature observed for Au@Pd than the bare Au nanoparticles (Figure S12).

Based on the above findings, a three-step mechanism for the transmission of hot electrons was proposed here (Figure 4D). Hot electrons are first generated at the Au cores under the excitation of incident light, and their energy is dependent on the wavelength of the incident light. To participate in the photocatalytic conversion of pATP, the hot electrons need to transfer across the interface between the Au core and the shell then go into the shell. After that, the hot electrons would migrate in the shell and arrive at its surface to trigger the conversion of pATP to DMAB. For the Au-insulator (Au-SiO_2) interface, the energy of the conduction band of the insulator overlayer is so high that the photogenerated hot electrons cannot transfer across

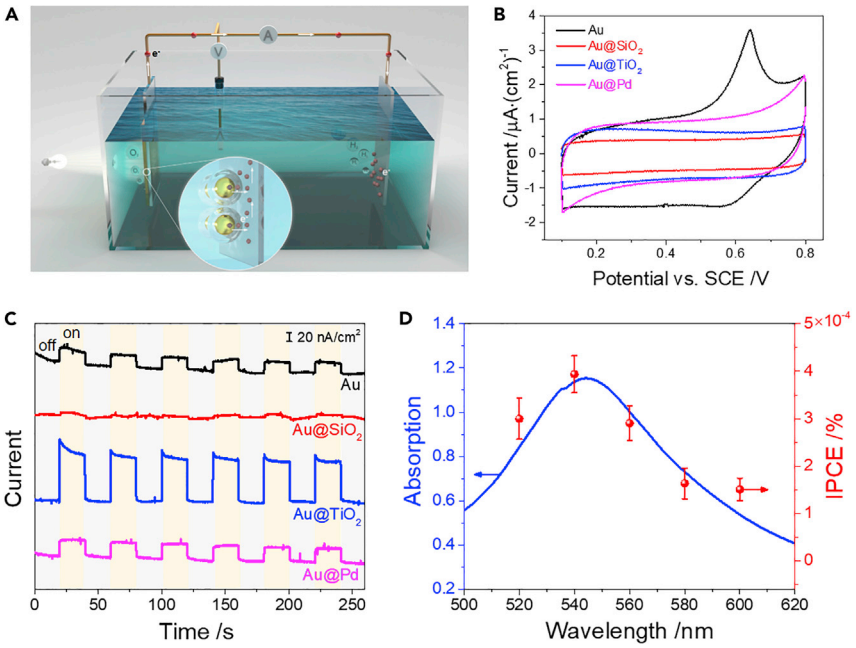

Figure 5. Photoelectrochemical Water Splitting Using the Plasmonic Core-Shell Nanoparticles

(A) Schematic diagram of photoelectrochemical water splitting using core-shell nanoparticles as the working electrode.

(B) Cyclic voltammograms of bare Au nanoparticles and core-shell nanoparticles.

(C) Amperometric i-t curves of bare Au nanoparticles and core-shell nanoparticles at 0.7 V versus SCE.

(D) Incident photon-to-electron conversion efficiencies at different wavelengths of Au@TiO_2 at 1.0 V versus SCE and the UV-vis spectrum of Au@TiO_2.

the Au-insulator interface and are thus insulated from reacting with pATP. For the Au-metal (Au-Pd or Au-Pt) interface, the hot electrons can be transferred into the Pd or Pt shell via the Au-metal interface but their lifetime in metal is much shorter due to the continuous electronic band structure of metal. Therefore, the hot electrons can only travel a very short distance in metals (<1 nm). As for the Au-semiconductor (Au-TiO_2 or Au-Cu_2O) interface, the conduction band of the semiconductor overlayer locates near the Au Fermi level so that the hot electrons can be easily transferred to the semiconductor shell via the Au-semiconductor interface. At the same time, due to the Schottky barrier, the hot electrons have a long lifetime in semiconductors. Consequently, hot electrons can penetrate very thick semiconductor shells (> 10 nm) and trigger photocatalytic reactions on the surface.

Photoelectrochemical Water Splitting Using the Plasmonic Core-Shell Nanoparticles

To further confirm the interfacial hot-electron transfer mechanism and expand it to more practical systems besides the above model reaction of pATP to DMAB, the plasmonic core-shell nanoparticles with different shell materials are then applied in the photoelectrochemical water splitting. As is well known, the photoelectrochemical water splitting is one of the most important reactions in the energy field and a promising way for sustainable H^2 generation. In such a photoelectrochemical system, the bare Au nanoparticles or core-shell nanoparticles with 2 nm shells are used as the working electrode. The hot electrons generated in the bare Au or core-shell nanoparticles flow to the Pt counter electrode via the external circuit and drive the hydrogen evolution reaction (HER) there (Figure 5A). The cyclic

voltammogram of bare Au nanoparticles displays a strong oxidation peak at around 0.65 V_{SCE} (Figure 5B), which can be assigned to the oxidation of the Au surface. Such a peak completely disappears for Au@SiO_2, Au@TiO_2, and Au@Pd, indicating that the Au surface has been fully covered by SiO_2, TiO_2, and Pd, respectively, in these core-shell nanoparticles.

Figure 5C shows the amperometric i-t curves of the bare Au nanoparticles and different core-shell nanoparticles at a constant potential of 0.7 V_{SCE}. A prompt and reproducible photocurrent can be clearly observed for the bare Au nanoparticles. Such a photocurrent almost completely disappears for the Au@SiO_2 core-shell nanoparticles. This result further confirms that the silica shells can block the transfer of hot electrons, which is well consistent with the finding in plasmon-mediated conversion of pATP to DMAB. Similar photoresponse has been observed for Au@Pd. This is very different from the result of the photocatalytic conversion of pATP, which shows that Au@Pd cannot catalyze the conversion of pATP to DMAB. As discussed before, hot electrons can be transferred from Au to Pd via the Au-Pd interface but the lifetime of hot electrons in Pd is very short. Thus, they would decay to thermally equilibrated states in less than 1 nm and cannot participate in the photocatalytic conversion of pATP. However, in photoelectrochemical water splitting, the bias voltage in the external circuit can drive the separation of hot electrons and holes thus prolong the lifetime of hot electrons. Therefore, hot electrons can go further distances in Pd under such a circumstance and take part in the HER reaction in the counter electrode, leading to the observed photocurrent of Au@Pd.

As for Au@TiO_2, much higher photocurrent is also observed (Figure 5C) and the photocurrent at 0.7 and 1.0 V is about 1.8 and 2.4 times higher than the dark current (Figure S13). The better performance of Au@TiO_2 compared to bare Au nanoparticles should result from the Schottky barrier between Au and TiO_2, which further promotes the separation of hot electrons and holes. Moreover, the incident photon-to-electron conversion efficiencies at different wavelengths match well with the UV-vis spectrum of Au@TiO_2 and display a maximum value at the plasmonic band of Au (Figure 5D). Such results directly demonstrate that the enhanced photoelectrochemical performance results from the plasmonic effect of Au nanoparticles and further confirm that hot electrons can migrate across the Au-TiO_2 interfaces and transfer through the TiO_2 shell. Therefore, it can be anticipated that the fundamental mechanism for the interfacial hot-electron transfer reported here may also apply to other plasmon-enhanced photocatalytic processes.

In summary, the transmission of hot electrons at plasmonic interfaces was studied with a (sub)nanometer spatial resolution using *in situ* SERS and DFT herein. Core-shell nanoparticles consisting of Au cores and different shells including SiO_2, TiO_2 (and Cu_2O), and Pd (and Pt) as representative examples for insulators, semiconductors, and metals, respectively, were prepared and deposited on a Au(111) single crystal surfaces. Between the Au(111) surface and core-shell nanoparticles, a monolayer of pATP was adsorbed on the Au(111), forming a model sandwich gap-mode structure. Combined *in situ* SERS and DFT calculations and the transmission of hot electrons in these insulators, semiconductors, and metals was then studied using the photocatalytic conversion of pATP to DMAB as a probe reaction. It was demonstrated that the hot electrons generated by the Au nanoparticles could transfer from Au to semiconductors (TiO_2 and Cu_2O) via the Au-semiconductor interfaces and migrate in the semiconductors for a long distance (>6 nm in TiO_2 and >10 nm in Cu_2O) to its shell surface to participate in photocatalytic reactions. Such an interfacial hot-electron transfer process would also proceed at the Au-metal (Au-Pd or

Au-Pt) interfaces, but the hot electrons decayed to a thermally equilibrated state after entering these metals when the shell thickness was > 1 nm because of the continuous electronic band structure of these metals. However, the transmission of hot electrons was blocked at the Au-insulator (Au-SiO_2) interface due to the high conduction band of insulators, thus the photocatalytic coupling of pATP to DMAB was inhibited. Such fundamental findings are also supported by the results of photoelectrochemical water splitting using these core-shell nanoparticles. This work deepens the fundamental understanding on the mechanism of the transmission of hot electrons at plasmonic interfaces and promotes the design of highly efficient plasmon-enhanced photocatalysts.

EXPERIMENTAL PROCEDURES

Synthesis and Characterization

Au nanoparticles were prepared according to the Frens' method,[54] and the size of the Au nanoparticles were tuned by changing the amount of the sodium citrate solution. For the synthesis of Au nanoparticles with a size of 80 and 120 nm, a seed-mediated method was employed (see the Supplemental Information for details). Then, SiO_2, TiO_2, Cu_2O, Pd, and Pt shells were coated on the Au nanoparticles to generate the Au@SiO_2, Au@TiO_2, Au@Cu_2O, Au@Pd, and Au@Pt core-shell nanoparticles, respectively. Au@SiO_2 nanoparticles were prepared according to our previous report by the hydrolysis of sodium silicate in the presence of (3-aminopropyl) trimethoxysilane (APTMS) as the coupling agent.[46] Au@TiO_2 was synthesized by the hydrolysis of titanium (IV) (triethanolaminato) isopropoxide (TTIP) in isopropyl alcohol, and the shell thickness was controlled by changing the amount of TTIP and water. Au@Cu_2O was prepared by the reduction of $CuSO_4$ with ascorbic acid under alkaline conditions. Au@Pd or Au@Pt was obtained by reducing H_2PdCl_4 or H_2PtCl_6 on the as-prepared Au sols using ascorbic acid as the reducing agent. Au-core Pd-satellite nanocomposites were prepared using a charge-induced self-assembly method.[55,56] For the detailed synthetic procedure, please refer to the Supplemental Information. The morphology and composition of the nanoparticles was characterized by HR-TEM coupled with energy dispersive X-ray spectrometry using a FEI Tecnai F30 microscope.

SERS Measurement

The Au(111) single crystal surface was prepared via the Clavilier method.[57] The freshly prepared Au(111) single crystal surface was immersed in a 1 mM pATP solution for 5 h. It was then thoroughly washed with ethanol to remove the physically adsorbed molecules, allowing the formation of a monolayer of pATP on Au(111). ~10 μL concentrated Au nanoparticles or core-shell nanoparticles were then deposited on the pATP assembled Au(111). The sample was naturally dried before the Raman measurement. Raman measurements were carried out on a Jobin Yvon Horiba Xplora confocal Raman system with a ×50 microscope objective. A 633 nm laser was used as the excitation light. All the Raman measurements, unless special instruction was given, were performed at 20°C.

Photoelectrochemical Measurements

All the electrochemical and photoelectrochemical experiments were carried out in a three-electrode system. The bare Au nanoparticles and core-shell nanoparticles were fabricated to two-dimensional metal nanoparticle arrays on ITO substrates via a two-phase method,[58] which was used as the working electrode in the measurements. A platinum sheet and a saturated calomel electrode (SCE) were used as the counter electrode and the reference electrode, respectively. 0.1 M Na_2SO_4 aqueous solution was used as the electrolyte.

Computational Method

All density functional theory (DFT) calculations were performed using the Vienna *ab initio* simulation package (VASP). The projector augmented potential (PAW) method[59] was implemented. The Perdew-Burker-Ernzerhof (PBE)[60] functional at the generalized gradient approximation (GGA) level was used, and the plane wave basis set was cut off at the energy of 450 eV. The Methfessel-Paxton method was employed to speed up the wave functional convergence with an electronic temperature of 0.1 eV. The quasi-Newton scheme was used in geometry optimization and convergence criterion for the force was set at less than 0.02 eV/Å for all calculations. The calculated lattice constant of Au bulk was 4.159 Å. The Au surface was modeled using a five layers 2×2 Au(111) slab with the bottom 2 layers fixed. The slab and its image were separated by a vacuum region of 20 Å. Pd, anatase TiO_2, and quartz SiO_2 overlayers were covered on the Au(111) surface to simulate the corresponding interfacial structures. The Γ-centered k-point sampling grid of 6 × 6 × 1 was adopted for geometric optimization. For the calculation of density of states (DOS), the k-point sampling grid was increased to 18 × 18 × 1.

SUPPLEMENTAL INFORMATION

Supplemental Information can be found online at https://doi.org/10.1016/j.chempr.2019.12.015.

ACKNOWLEDGMENTS

This work was supported by the National Natural Science Foundation of China (NSFC) (21703181, 21972117, 21925404, 21775127, 21427813, and 21673187), the Fundamental Research Funds for the Central Universities (20720190044 and 20720190018), and the State Key Laboratory of Fine Chemicals (KF1702). We thank Prof. M. Moskovits for helpful discussions and Y.H. Wang and T.M. Chen for experimental support.

AUTHOR CONTRIBUTIONS

H.Z. and J.-F.L. developed the project and designed the experiments. H.Z., J.W., and Y.-J.Z. carried out the experiments. X.-G.Z. and D.-Y.W. conducted the DFT simulations. H.Z., P.M.R., F.P., Z.-Q.T., and J.-F.L. analyzed the data. All authors contributed to the preparation of the manuscript.

DECLARATION OF INTERESTS

The authors declare no competing interests.

Received: June 22, 2019
Revised: September 26, 2019
Accepted: December 12, 2019
Published: January 9, 2020

REFERENCES

1. Fujishima, A., and Honda, K. (1972). Electrochemical photolysis of water at a semiconductor electrode. Nature *238*, 37–38.

2. Chen, S., Takata, T., and Domen, K. (2017). Particulate photocatalysts for overall water splitting. Nat. Rev. Mater. *2*, 17050.

3. Wang, Q., Hisatomi, T., Jia, Q., Tokudome, H., Zhong, M., Wang, C., Pan, Z., Takata, T., Nakabayashi, M., Shibata, N., et al. (2016). Scalable water splitting on particulate photocatalyst sheets with a solar-to-hydrogen energy conversion efficiency exceeding 1%. Nat. Mater. *15*, 611–615.

4. Cargnello, M., Montini, T., Smolin, S.Y., Priebe, J.B., Delgado Jaén, J.J., Doan-Nguyen, V.V.T., McKay, I.S., Schwalbe, J.A., Pohl, M.M., Gordon, T.R., et al. (2016). Engineering titania nanostructure to tune and improve its photocatalytic activity. Proc. Natl. Acad. Sci. USA *113*, 3966–3971.

5. Tian, B., Tian, B., Smith, B., Scott, M.C., Hua, R., Lei, Q., and Tian, Y. (2018). Supported black phosphorus nanosheets as hydrogen-evolving photocatalyst achieving 5.4% energy conversion efficiency at 353 K. Nat. Commun. *9*, 1397.

6. Brongersma, M.L., Halas, N.J., and Nordlander, P. (2015). Plasmon-induced hot carrier science and technology. Nat. Nanotechnol. *10*, 25–34.

7. Linic, S., Aslam, U., Boerigter, C., and Morabito, M. (2015). Photochemical

transformations on plasmonic metal nanoparticles. Nat. Mater. *14*, 567–576.

8. Zhang, N., Han, C., Fu, X., and Xu, Y.J. (2018). Function-oriented engineering of metal-based nanohybrids for photoredox catalysis: exerting plasmonic effect and beyond. Chem *4*, 1832–1861.

9. Christopher, P., and Moskovits, M. (2017). Hot charge carrier transmission from plasmonic nanostructures. Annu. Rev. Phys. Chem. *68*, 379–398.

10. Atta, S., Pennington, A.M., Celik, F.E., and Fabris, L. (2018). TiO_2 on gold nanostars enhances photocatalytic water reduction in the near-infrared regime. Chem *4*, 2140–2153.

11. Mukherjee, S., Zhou, L., Goodman, A.M., Large, N., Ayala-Orozco, C., Zhang, Y., Nordlander, P., and Halas, N.J. (2014). Hot-electron-induced dissociation of H_2 on gold nanoparticles supported on SiO_2. J. Am. Chem. Soc. *136*, 64–67.

12. Christopher, P., Xin, H., and Linic, S. (2011). Visible-light-enhanced catalytic oxidation reactions on plasmonic silver nanostructures. Nat. Chem. *3*, 467–472.

13. Xiao, Q., Liu, Z., Bo, A., Zavahir, S., Sarina, S., Bottle, S., Riches, J.D., and Zhu, H.Y. (2015). Catalytic transformation of aliphatic alcohols to corresponding esters in O_2 under neutral conditions using visible-light irradiation. J. Am. Chem. Soc. *137*, 1956–1966.

14. Al-Zubeidi, A., Hoener, B.S., Collins, S.S.E., Wang, W., Kirchner, S.R., Hosseini Jebeli, S.A., Joplin, A., Chang, W.S., Link, S., and Landes, C.F. (2019). Hot holes assist plasmonic nanoelectrode dissolution. Nano Lett. *19*, 1301–1306.

15. Tanaka, A., Hashimoto, K., and Kominami, H. (2014). Visible-light-induced hydrogen and oxygen formation over $Pt/Au/WO_3$ photocatalyst utilizing two types of photoabsorption due to surface plasmon resonance and band-gap excitation. J. Am. Chem. Soc. *136*, 586–589.

16. Hao, C.H., Guo, X.N., Pan, Y.T., Chen, S., Jiao, Z.F., Yang, H., and Guo, X.Y. (2016). Visible-light-driven selective photocatalytic hydrogenation of cinnamaldehyde over Au/SiC catalysts. J. Am. Chem. Soc. *138*, 9361–9364.

17. Mubeen, S., Lee, J., Singh, N., Krämer, S., Stucky, G.D., and Moskovits, M. (2013). An autonomous photosynthetic device in which all charge carriers derive from surface plasmons. Nat. Nanotechnol. *8*, 247–251.

18. Wu, K., Chen, J., McBride, J.R., and Lian, T. (2015). CHARGE TRANSFER. Efficient hot-electron transfer by a plasmon-induced interfacial charge-transfer transition. Science *349*, 632–635.

19. Tanabe, I., and Ozaki, Y. (2014). Consistent changes in electronic states and photocatalytic activities of metal (Au, Pd, Pt)-modified TiO_2 studied by far-ultraviolet spectroscopy. Chem. Commun. (Camb.) *50*, 2117–2119.

20. Wang, F., Li, C., Chen, H., Jiang, R., Sun, L.D., Li, Q., Wang, J., Yu, J.C., and Yan, C.H. (2013). Plasmonic harvesting of light energy for Suzuki coupling reactions. J. Am. Chem. Soc. *135*, 5588–5601.

21. Zheng, Z., Tachikawa, T., and Majima, T. (2015). Plasmon-enhanced formic acid dehydrogenation using anisotropic Pd–Au nanorods studied at the single-particle level. J. Am. Chem. Soc. *137*, 948–957.

22. Kale, M.J., Avanesian, T., Xin, H., Yan, J., and Christopher, P. (2014). Controlling catalytic selectivity on metal nanoparticles by direct photoexcitation of adsorbate–metal bonds. Nano Lett. *14*, 5405–5412.

23. Kochuveedu, S.T., Jang, Y.H., and Kim, D.H. (2013). A study on the mechanism for the interaction of light with noble metal-metal oxide semiconductor nanostructures for various photophysical applications. Chem. Soc. Rev. *42*, 8467–8493.

24. Cushing, S.K., Li, J., Meng, F., Senty, T.R., Suri, S., Zhi, M., Li, M., Bristow, A.D., and Wu, N. (2012). Photocatalytic activity enhanced by plasmonic resonant energy transfer from metal to semiconductor. J. Am. Chem. Soc. *134*, 15033–15041.

25. Robatjazi, H., Bahauddin, S.M., Doiron, C., and Thomann, I. (2015). Direct plasmon-driven photoelectrocatalysis. Nano Lett. *15*, 6155–6161.

26. Lee, Y.K., Jung, C.H., Park, J., Seo, H., Somorjai, G.A., and Park, J.Y. (2011). Surface plasmon-driven hot electron flow probed with metal-semiconductor nanodiodes. Nano Lett. *11*, 4251–4255.

27. Zhang, Z., Liu, L., Fang, W.H., Long, R., Tokina, M.V., and Prezhdo, O.V. (2018). Plasmon-mediated electron injection from Au nanorods into MoS_2: traditional versus photoexcitation mechanism. Chem *4*, 1112–1127.

28. Clavero, C. (2014). Plasmon-induced hot-electron generation at nanoparticle/metal-oxide interfaces for photovoltaic and photocatalytic devices. Nat. Photonics *8*, 95–103.

29. Li, Y., Hu, Y., Shi, F., Li, H., Xie, W., and Chen, J. (2019). C–H arylation on nickel nanoparticles monitored by in situ surface-enhanced Raman spectroscopy. Angew. Chem. Int. Ed. Engl. *58*, 9049–9053.

30. Li, C.Y., Le, J.B., Wang, Y.H., Chen, S., Yang, Z.L., Li, J.F., Cheng, J., and Tian, Z.Q. (2019). In situ probing electrified interfacial water structures at atomically flat surfaces. Nat. Mater. *18*, 697–701.

31. Hoener, B.S., Kirchner, S.R., Heiderscheit, T.S., Collins, S.S.E., Chang, W.S., Link, S., and Landes, C.F. (2018). Plasmonic sensing and control of single-nanoparticle electrochemistry. Chem *4*, 1560–1585.

32. Cortés, E., Xie, W., Cambiasso, J., Jermyn, A.S., Sundararaman, R., Narang, P., Schlücker, S., and Maier, S.A. (2017). Plasmonic hot electron transport drives nano-localized chemistry. Nat. Commun. *8*, 14880.

33. Huang, Y.F., Zhu, H.P., Liu, G.K., Wu, D.Y., Ren, B., and Tian, Z.Q. (2010). When the signal is not from the original molecule to be detected: chemical transformation of para-aminothiophenol on Ag during the SERS measurement. J. Am. Chem. Soc. *132*, 9244–9246.

34. Kumar, N., Wondergem, C.S., Wain, A.J., and Weckhuysen, B.M. (2019). In situ nanoscale investigation of catalytic reactions in the liquid phase using zirconia-protected tip-enhanced Raman spectroscopy probes. J. Phys. Chem. Lett. *10*, 1669–1675.

35. Cui, K., Fan, C., Chen, G., Qiu, Y., Li, M., Lin, M., Wan, J.B., Cai, C., and Xiao, Z. (2018). para-Aminothiophenol radical reaction-functionalized gold nanoprobe for one-to-all detection of five reactive oxygen species in vivo. Anal. Chem. *90*, 12137–12144.

36. van Schrojenstein Lantman, E.M., Deckert-Gaudig, T., Mank, A.J.G., Deckert, V., and Weckhuysen, B.M. (2012). Catalytic processes monitored at the nanoscale with tip-enhanced Raman spectroscopy. Nat. Nanotechnol. *7*, 583–586.

37. Si, S., Liang, W., Sun, Y., Huang, J., Ma, W., Liang, Z., Bao, Q., and Jiang, L. (2016). Facile fabrication of high-density sub-1-nm gaps from Au nanoparticle monolayers as reproducible SERS substrates. Adv. Funct. Mater. *26*, 8137–8145.

38. Reguera, J., Langer, J., Jiménez de Aberasturi, D., and Liz-Marzán, L.M. (2017). Anisotropic metal nanoparticles for surface enhanced Raman scattering. Chem. Soc. Rev. *46*, 3866–3885.

39. Zhang, Z., Merk, V., Hermanns, A., Unger, W.E.S., and Kneipp, J. (2017). Role of metal cations in plasmon-catalyzed oxidation: a case study of p-aminothiophenol dimerization. ACS Catal. *7*, 7803–7809.

40. Almohammed, S., Tade Barwich, S., Mitchell, A.K., Rodriguez, B.J., and Rice, J.H. (2019). Enhanced photocatalysis and biomolecular sensing with field-activated nanotube-nanoparticle templates. Nat. Commun. *10*, 2496.

41. Wang, J., Ando, R.A., and Camargo, P.H.C. (2015). Controlling the selectivity of the surface plasmon resonance mediated oxidation of p-aminothiophenol on Au nanoparticles by charge transfer from UV-excited TiO_2. Angew. Chem. Int. Ed. Engl. *54*, 6909–6912.

42. Huang, Y.F., Zhang, M., Zhao, L.B., Feng, J.M., Wu, D.Y., Ren, B., and Tian, Z.Q. (2014). Activation of oxygen on gold and silver nanoparticles assisted by surface plasmon resonances. Angew. Chem. Int. Ed. Engl. *53*, 2353–2357.

43. Yan, X., Wang, L., Tan, X., Tian, B., and Zhang, J. (2016). Surface-enhanced Raman spectroscopy assisted by radical capturer for tracking of plasmon-driven redox reaction. Sci. Rep. *6*, 30193.

44. Liebig, F., Sarhan, R.M., Sander, M., Koopman, W., Schuetz, R., Bargheer, M., and Koetz, J. (2017). Deposition of gold nanotriangles in large scale close-packed monolayers for X-ray-based temperature calibration and SERS monitoring of plasmon-driven catalytic reactions. ACS Appl. Mater. Interfaces *9*, 20247–20253.

45. Sarhan, R.M., Koopman, W., Schuetz, R., Schmid, T., Liebig, F., Koetz, J., and Bargheer, M. (2019). The importance of plasmonic heating for the plasmon-driven

photodimerization of 4-nitrothiophenol. Sci. Rep. *9*, 3060.

46. Li, J.F., Huang, Y.F., Ding, Y., Yang, Z.L., Li, S.B., Zhou, X.S., Fan, F.R., Zhang, W., Zhou, Z.Y., Wu, D.Y., et al. (2010). Shell-isolated nanoparticle-enhanced Raman spectroscopy. Nature *464*, 392–395.

47. Zhang, Y.J., Li, S.B., Duan, S., Lu, B.A., Yang, J., Panneerselvam, R., Li, C.Y., Fang, P.P., Zhou, Z.Y., Phillips, D.L., et al. (2016). Probing the electronic structure of heterogeneous metal interfaces by transition metal shelled gold nanoparticle-enhanced Raman spectroscopy. J. Phys. Chem. C *120*, 20684–20691.

48. Zhang, H., Zhang, X.G., Wei, J., Wang, C., Chen, S., Sun, H.L., Wang, Y.H., Chen, B.H., Yang, Z.L., Wu, D.Y., et al. (2017). Revealing the role of interfacial properties on catalytic behaviors by *in situ* surface-enhanced Raman spectroscopy. J. Am. Chem. Soc. *139*, 10339–10346.

49. Dong, Y., Su, Y., Du, L., Wang, R., Zhang, L., Zhao, D., and Xie, W. (2019). Plasmon-enhanced deuteration under visible-light irradiation. ACS Nano *13*, 10754–10760.

50. Zhong, J.H., Jin, X., Meng, L., Wang, X., Su, H.S., Yang, Z.L., Williams, C.T., and Ren, B. (2017). Probing the electronic and catalytic properties of a bimetallic surface with 3 nm resolution. Nat. Nanotechnol. *12*, 132–136.

51. Zheng, Z., Tachikawa, T., and Majima, T. (2014). Single-particle study of Pt-modified Au nanorods for plasmon-enhanced hydrogen generation in visible to near-infrared region. J. Am. Chem. Soc. *136*, 6870–6873.

52. Chavez, S., Aslam, U., and Linic, S. (2018). Design principles for directing energy and energetic charge flow in multicomponent plasmonic nanostructures. ACS Energy Lett. *3*, 1590–1596.

53. Park, J.Y., Baker, L.R., and Somorjai, G.A. (2015). Role of hot electrons and metal–oxide interfaces in surface chemistry and catalytic reactions. Chem. Rev. *115*, 2781–2817.

54. Frens, G. (1973). Controlled nucleation for the regulation of the particle size in monodisperse gold suspensions. Nature *241*, 20–22.

55. Wang, C., Chen, X., Chen, T.M., Wei, J., Qin, S.-N., Zheng, J.F., Zhang, H., Tian, Z.Q., and Li, J.F. (2019). In-situ SHINERS study of the size and composition effect of Pt-based nanocatalysts in catalytic hydrogenation. ChemCatChem. Published online October 30, 2019. https://doi.org/10.1002/cctc.201901747.

56. Wang, Y.H., Le, J.B., Li, W.Q., Wei, J., Radjenovic, P.M., Zhang, H., Zhou, X.S., Cheng, J., Tian, Z.Q., and Li, J.F. (2019). In situ spectroscopic insight into the origin of the enhanced performance of bimetallic nanocatalysts towards oxygen reduction reaction (ORR). Angew. Chem. Int. Ed. Engl. *58*, 16062–16066.

57. Clavilier, J., Faure, R., Guinet, G., and Durand, R. (1980). Preparation of monocrystalline Pt microelectrodes and electrochemical study of the plane surfaces cut in the direction of the {111} and {110} planes. J. Electroanal. Chem. Interfacial Electrochem. *107*, 205–209.

58. Xu, Y., Konrad, M.P., Lee, W.W.Y., Ye, Z., and Bell, S.E.J. (2016). A method for promoting assembly of metallic and nonmetallic nanoparticles into interfacial monolayer films. Nano Lett. *16*, 5255–5260.

59. Blöchl, P.E. (1994). Projector augmented-wave method. Phys. Rev. B Condens. Matter *50*, 17953–17979.

60. Perdew, J.P., Burke, K., and Ernzerhof, M. (1996). Generalized gradient approximation made simple. Phys. Rev. Lett. *77*, 3865–3868.